

## ENDOR of Spin-Correlated Radical Pairs in Photosynthesis at High Magnetic Field: A Tool for Mapping Electron Transfer Pathways

Oleg G. Poluektov,<sup>\*,†</sup> Lisa M. Utschig,<sup>†</sup> Alexander A. Dubinskij,<sup>‡</sup> and Marion C. Thurnauer<sup>†</sup>

Chemistry Division, Argonne National Laboratory, 9700 South Cass Avenue, Argonne, Illinois 60439, and  
Institute of Chemical Physics, Russian Academy of Sciences, Kosygina 4, Moscow 117977, Russia

Received October 29, 2003; E-mail: Oleg@anl.gov

In photosynthesis, the primary energy conversion reactions involve a photoinitiated sequence of efficient electron-transfer steps resulting in charge separation across a biological membrane, thus converting light into an electrochemical potential.<sup>1</sup> These reactions occur between cofactors held within integral membrane reaction center (RC) proteins. Figure 1 shows the arrangement of cofactors in the purple photosynthetic bacterial RC, with arrows indicating the pathways and kinetics of sequential electron-transfer steps that result in the charge-separated state  $P^+Q_A^-$ , where the primary electron donor P is a pair of bacteriochlorophyll molecules and the secondary electron acceptor  $Q_A$  is a quinone molecule.<sup>1</sup>

Time-resolved (TR) EPR spectroscopy has been extensively used to monitor the primary photochemistry in RCs of purple bacteria and photosystems I and II of cyanobacteria and green plants.<sup>2</sup> The TR-EPR spectra of the transient intermediates exhibit electron spin polarization (ESP), i.e., a non-Boltzmann spin population distribution. Importantly, ESP is sensitive to the magnetic resonance parameters and interactions between photochemically oxidized and reduced species, thereby revealing structure and dynamics of the photoactive RC. For example, the ESP exhibited by  $P^+Q_A^-$  is explained by the spin-correlated radical pair (SCRPA) model.<sup>2,3</sup> In this context, the photosynthetic RCs continue to provide a fascinating “playground” for the development of advanced theoretical and experimental approaches in magnetic resonance, which, in turn, provide insight into the charge separation process. On the basis of the SCRPA model, several spin phenomena have been explained and/or predicted, such as quantum beats observed at short delay times after optical excitation;<sup>4</sup> out-of-phase modulation of the electron spin echo (ESE) signal, which is due to dipole–dipole and exchange interactions in the SCRPA and allows for distance measurements;<sup>5</sup> multiple quantum coherence in photoinduced radical pairs, which allows for direct measurements of coherence decays;<sup>6</sup> and sequential electron-transfer polarization mechanism, which allows for study of the electron-transfer dynamics.<sup>7</sup>

Here we report on a new phenomenon, which is associated with the SCRPA model. This phenomenon is manifest when TR electron–nuclear double resonance (ENDOR) spectra of photosynthetic RC proteins are recorded at high magnetic field (HF) EPR ( $>3$  T). The HF-ENDOR spectra of the SCRPA reveal a derivative-like, complicated line shape, which differs considerably from the ENDOR spectra of chemically reduced  $Q_A$ . This phenomenon can be explained within the SCRPA model by taking into account hyperfine interactions (HFI) of a particular nucleus with both radicals in the SCRPA. Thus, SCRPA ENDOR has the potential for mapping the overlap of electronic wave functions of the donor and acceptor in the protein environment. This will lead to a better understanding of the electron-transfer pathways in the photosyn-

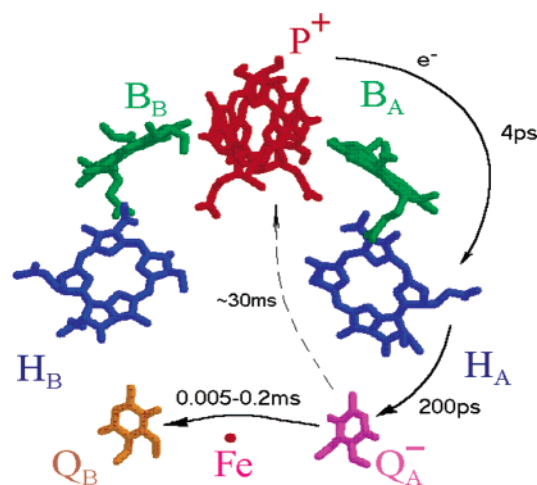


**Figure 1.** Arrangement of cofactors of the RC from *Rb. sphaeroides* as revealed by X-ray crystallography.<sup>1</sup> For clarity, protein matrix is not shown. P is a pair of bacteriochlorophyll (Bchl) molecules,  $B_A$  and  $B_B$  are so-called accessory Bchl's,  $H_A$  and  $H_B$  are bacteriopheophytin, and  $Q_A$  and  $Q_B$  are ubiquinones situated around non-heme Fe ion. The pathways and time constants of the rapid sequential transfer steps are indicated by arrows. At low temperatures, electron transfer from  $Q_A^-$  to  $Q_B$  is blocked, and the electron on  $Q_A^-$  returns to  $P^+$  (dashed arrow).

thetic RC proteins and, in particular, of how the protein environment controls electron-transfer reactions.

The effect has been observed in Fe-removed/Zn-replaced bacterial RC proteins from protonated ( $^1H$ ) *Rhodobacter sphaeroides*<sup>8</sup> in which  $Q_A$  is deuterated ( $^2H$ ) ubiquinone-10. EPR and ENDOR measurements were performed on a pulsed/continuous wave high-frequency D-band (130GHz/4.6T) EPR spectrometer.<sup>9</sup> Light excitation was achieved with an optical parametric oscillator (Opotek) pumped by a Nd:YAG laser (Quantel), the output of which was coupled to a fiber optic that delivered light to the sample. Pulsed TR-EPR spectra of the SCRPA were recorded by monitoring the electron spin echo (ESE) from a two-microwave (MW) pulse sequence, which followed a 10-ns laser pulse at a fixed delay time ( $D_t$ ), as a function of magnetic field. Pulsed ENDOR spectra were recorded using a Mims-type<sup>10</sup> sequence of MW and radio frequency (RF) pulses (laser –  $D_t$  –  $\pi/2_{MW}$  –  $\tau$  –  $\pi/2_{MW}$  –  $\pi_{RF}$  –  $\pi/2_{MW}$ ) by monitoring the ESE intensity as a function of the frequency of the RF pulse. Additional experimental conditions are described in the Figure 2 caption.

HF-EPR spectra of the chemically reduced deuterated  $Q_A$  (superimposed with a spectrum of protonated  $P^+$ ) and SCRPA  $P^+Q_A^-$  are shown in Figure 2a,b, respectively. At HF the  $g$ -tensor of  $Q_A^-$  is well-resolved and exhibits spectral turning points for each of its three main axes. Therefore, ENDOR spectra can be recorded at magnetic field positions within the  $Q_A^-$  spectral domain which are well-separated from that of  $P^+$  and are at a particular orientation

<sup>†</sup> Argonne National Laboratory.

<sup>‡</sup> Russian Academy of Sciences.

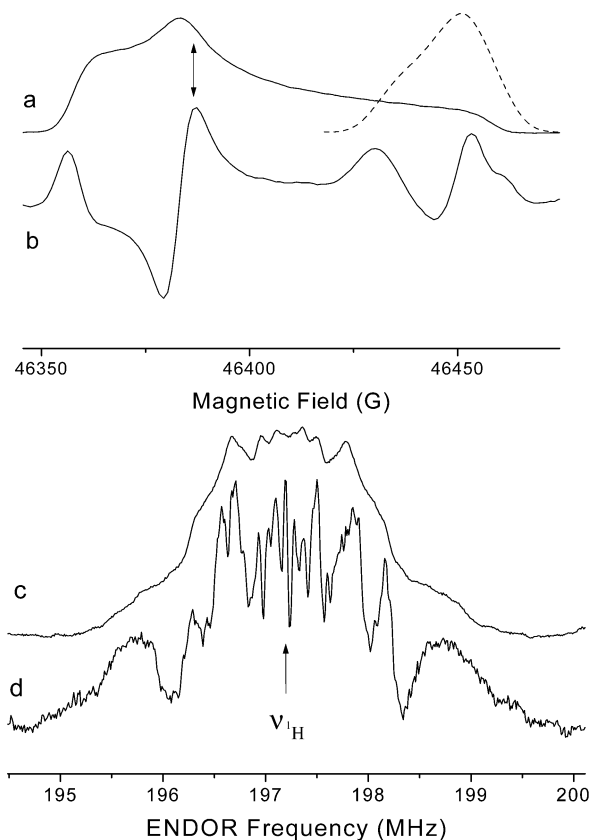


**Figure 2.** (a,b) Magnetic field-swept ESE and (c,d) Mims-type  $^1\text{H}$  ENDOR spectra of Fe-removed/Zn-substituted photosynthetic bacterial RC with deuterated  $\text{Q}_\text{A}$ , recorded at D-band EPR,  $T = 50$  K. (a,c) Spectra of chemically reduced  $\text{Q}_\text{A}$ , with superimposed protonated  $\text{P}^+$  spectrum (dashed line on a). (b,d) Spectra of SCR  $\text{P}^+\text{Q}_\text{A}^-$ , recorded with  $D_\text{t} = 2 \mu\text{s}$ ,  $\pi/2_{\text{MW}} = 50$  ns,  $\tau = 200$  ns, laser excitation  $\lambda = 550$  nm. For  $^1\text{H}$  ENDOR (c,d)  $\pi_{\text{RF}} = 20 \mu\text{s}$ . Arrow: (a,b) magnetic field position at which ENDOR spectra recorded and (c,d)  $^1\text{H}$  Larmor frequency.

of the  $\text{Q}_\text{A}^-$   $g$ -tensor. Such a position (indicated by arrow, Figure 2a,b) was selected for recording  $^1\text{H}$  ENDOR spectra (Figure 2c,d). The advantage of the Mims-type ENDOR is that it has superior sensitivity for nuclei with small HFI, thus allowing for observation of HFI with distant nuclei, e.g., from the protein environment, so-called matrix ENDOR.  $^1\text{H}$ -ENDOR performed at the  $\text{Q}_\text{A}^-$  EPR line is a pure matrix ENDOR with respect to this radical, because deuterated  $\text{Q}_\text{A}^-$  does not contain any protons (Figure 2c,d).

The SCR ENDOR spectrum recorded with  $D_\text{t}$  in the  $\mu\text{s}$  regime (Figure 2d) exhibits striking differences from that of chemically reduced  $\text{Q}_\text{A}$  (Figure 2c). The main features of the SCR ENDOR spectra are narrowing of the ENDOR lines, resulting in substantially increased spectral resolution, some lines appearing as derivatives of absorption lines, suppression of some sets of lines and amplification of others, and the SCR ENDOR spectra not being symmetric around the nuclear Larmor frequency, as in the case of ENDOR spectra of stable radicals (Figure 2c).

This observation is similar to the time-dependent behavior of SCR EPR spectra when recorded at high magnetic field (see Figure 2a,b). The better resolution of the HF EPR SCR spectra and their derivative line shapes (Figure 2b) compared to the equilibrium spectra (Figure 2a) are well understood within an “interaction field” approach as presented in ref 11. The single EPR lines for each orientation of  $\text{Q}_\text{A}^-$  split into two with equal intensities and opposite phase (“emission and absorption”) due to dipole–dipole and

exchange interactions with the unpaired spin on  $\text{P}^+$ . The total line shape of the SCR EPR spectrum can be derived by integration of these absorptive and emissive lines over all orientations of the radical pair, which results in the derivative line shapes.

A similar effect leads to the derivative line shapes in the SCR ENDOR spectra. The position of the ENDOR lines in the SCR ENDOR spectrum (Figure 2d), recorded through the  $\text{Q}_\text{A}^-$  EPR signal, is determined by the HFI with the  $\text{Q}_\text{A}^-$  electron spin, while the HFI with  $\text{P}^+$  splits the lines into two with absorptive and emissive phases. Certainly, the SCR ENDOR spectra are more complex than that of SCR EPR, because there are many nuclei which contribute to the spectra and HFI with both radicals for these nuclei can differ considerably. This leads to the strong interference-type pattern. Importantly, the derivative line shapes and asymmetry in ENDOR can be observed only from the nuclei which have HFI with both unpaired electrons in the SCR.

The recently reported pulsed TR-ENDOR in photosystem I recorded at conventional X-band (9GHz/0.35T) EPR is also a consequence of ESP in SCR.<sup>12</sup> However, the spectral manifestation and physical explanation are different and can be understood by taking into account a nonselective excitation and effective mixing of  $|S\rangle$  and  $|T_0\rangle$  states at the low magnetic field of X-band EPR.<sup>12</sup>

In conclusion, we have reported a new effect observed in the HF TR-ENDOR spectra of the SCR in photosynthetic RC proteins. The SCR ENDOR contains data on spin density delocalization in the protein environment between the electron donor and acceptor in the SCR. Revealing this information will provide a unique opportunity to probe the electron-transfer pathways in natural and artificial photosynthetic assemblies.

**Acknowledgment.** Work at ANL was supported by the U.S. Dept. of Energy, Office of Basic Energy Sciences, Div. of Chemical Sciences, Geosciences, and Biosciences, Contract W-31-109-Eng-38.

## References

- (1) (a) *Photosynthetic Reaction Centers*; Deisenhofer, J., Norris, J. R., Eds.; Academic Press: New York, 1993; Vols. I, II. (b) Wright, C. A. *Front. Biosci.* **2004**, *9*, 309–337.
- (2) (a) Snyder, S. W.; Thurnauer, M. C. In *Photosynthetic Reaction Centers*; Deisenhofer, J., Norris, J. R., Eds.; Academic Press: New York, 1993; Vol. II, pp 285–329. (b) Stehlik, D.; Möbius, K. *Annu. Rev. Phys. Chem.* **1997**, *48*, 745–784.
- (3) (a) Thurnauer, M. C.; Norris, J. R. *Chem. Phys. Lett.* **1980**, *76*, 557–561. (b) Closs, G. L.; Forbes, M. D. E.; Norris, J. R. *J. Phys. Chem.* **1987**, *91*, 3592–3599. (c) Buckley, C. D.; Hunter, D. A.; Hore, P. J.; McLauchlan, K. A. *Chem. Phys. Lett.* **1987**, *135*, 307–312.
- (4) (a) Salikhov, K. M.; Bock, C. H.; Stehlik, D. *Appl. Magn. Reson.* **1990**, *1*, 195–211. (b) Bittl, R.; Kothe, G. *Chem. Phys. Lett.* **1991**, *177*, 547–553. (c) Kothe, G.; Weber, S.; Bittl, R.; Ohmes, E.; Thurnauer, M. C.; Norris, J. R. *Chem. Phys. Lett.* **1991**, *186*, 474–480.
- (5) (a) Tang, J.; Thurnauer, M. C.; Norris, J. R. *Chem. Phys. Lett.* **1994**, *219*, 283–290. (b) Salikhov, K. M.; Kandrashkin, Yu. E.; Salikhov, A. K. *Appl. Magn. Reson.* **1992**, *3*, 199–216. (c) Dzuba, S. A.; Gast, P.; Hoff, A. J. *Chem. Phys. Lett.* **1995**, *236*, 595–602.
- (6) (a) Tang, J.; Norris, J. R. *Chem. Phys. Lett.* **1995**, *233*, 192–200. (b) Borovykh, I. V.; Kulik, L. V.; Dzuba, S. A.; Hoff, A. J. *Chem. Phys. Lett.* **2001**, *338*, 173–179.
- (7) (a) Norris, J. R.; Morris, A. L.; Thurnauer, M. C.; Tang, J. *J. Chem. Phys.* **1990**, *92*, 4239–4249. (b) Morris, A. L.; Snyder, S. W.; Zhang, Y.; Tang, J.; Thurnauer, M. C.; Dutton, P. L.; Robertson, D. E.; Gunner, M. R. *J. Phys. Chem.* **1995**, *99*, 3854–3866.
- (8) Utschig, L. M.; Greenfield, S. R.; Tang, J.; Laible, P. D.; Thurnauer, M. C. *Biochemistry* **1997**, *36*, 8548–8558.
- (9) Lakshmi, K. V.; Reifler, M. J.; Brudvig, G. W.; Poluektov, O. G.; Wagner, A. M.; Thurnauer, M. C. *J. Phys. Chem. B* **2000**, *104*, 10445.
- (10) Mims, W. B. *Proc. R. Soc. London* **1965**, *283*, 452.
- (11) Dubinski, A. A.; Perekhodtsev, G. D.; Poluektov, O. G.; Rajh, T.; Thurnauer, M. C. *J. Phys. Chem. B* **2002**, *106*, 938–944.
- (12) (a) Bittl, R.; Zech, S. G. *Biochim. Biophys. Acta* **2001**, *1507*, 194–211. (b) Fursman, C. E.; Teutloff, C.; Bittl, R. *J. Phys. Chem. B* **2002**, *106*, 9679–9686.

JA039309J